View metadata, citation and similar papers at core.ac.uk
brought to you by CORE
provided by PolyU Institutional Repository

AIP Applied Physics Letters

Tunable electronic transport properties of DyScO3/SrTiO3 polar heterointerface

D. F. Li, Yan Wang, and J. Y. Dai

Citation: Appl. Phys. Lett. **98**, 122108 (2011); doi: 10.1063/1.3570694
View online: http://dx.doi.org/10.1063/1.3570694
View Table of Contents: http://apl.aip.org/resource/1/APPLAB/v98/i12
Published by the American Institute of Physics.

Related Articles

Triboelectric charging of insulating polymers–some new perspectives
AIP Advances 2, 010701 (2012)

Influence of charge compensation mechanisms on the sheet electron density at conducting LaAlO3/SrTiO3-interfaces
Appl. Phys. Lett. 100, 052103 (2012)

Electrostatic carrier doping of GdTiO3/SrTiO3 interfaces
Appl. Phys. Lett. 99, 232116 (2011)

Laser-induced charging of microfabricated ion traps
J. Appl. Phys. 110, 104901 (2011)

Re-examining the properties of the aqueous vapor–liquid interface using dispersion corrected density functional theory
J. Chem. Phys. 135, 124712 (2011)

Additional information on Appl. Phys. Lett.

Journal Homepage: http://apl.aip.org/
Journal Information: http://apl.aip.org/about/about_the_journal
Top downloads: http://apl.aip.org/features/most_downloaded
Information for Authors: http://apl.aip.org/authors

ADVERTISEMENT

Downloaded 14 Feb 2012 to 158.132.161.192. Redistribution subject to AIP license or copyright; see http://apl.aip.org/about/rights_and_permissions

Tunable electronic transport properties of $DyScO_3/SrTiO_3$ polar heterointerface

D. F. Li, Yan Wang, and J. Y. Dai[a)]
Department of Applied Physics, The Hong Kong Polytechnic University, Hung Hom, Kowloon, Hong Kong

(Received 12 January 2011; accepted 5 March 2011; published online 24 March 2011)

Electronic transport properties of $DyScO_3/SrTiO_3$ polar heterointerface grown at different oxygen pressures are studied. This $DyScO_3/SrTiO_3$ polar heterointerface exhibits much higher charge mobility, up to 10^4 $cm^2\ V^{-1}\ s^{-1}$, compared to the $LaAlO_3/SrTiO_3$ system due to relatively lower lattice mismatch between the film and substrate. More significantly, the $DyScO_3$ film deposited under 10^{-4} mbar oxygen pressure presents an interfacial metal-to-semiconductor conducting mechanism transition at 90 K. Field effect transport measurement results reveal that this transition can be modulated by field effect through controlling the electron doping level of the interface originated from interfacial electronic reconstruction. © *2011 American Institute of Physics*.
[doi:10.1063/1.3570694]

Recently, study of perovskite heterointerfaces has attracted considerable interest due to the fact that unexpected physical properties, which are absent in either of the individual bulk constituents, may arise.[1,2] One prominent example is the discovery by Ohtomo and Hwang in 2004 (Ref. 3) of a high-mobility ($\sim 10^3$ $cm^2\ V^{-1}\ s^{-1}$ at 4.2 K) quasi-two-dimensional electron gas (q2-DEG) with high carrier density (10^{14} cm^{-2}) (Refs. 4–6) at heterointerfaces combining two band insulators $LaAlO_3$ (LAO) and $SrTiO_3$ (STO) making the interface conducting. Successively, numerous electronic properties have been deeply investigated at such interface, revealing superconducting[7] and intriguing magnetotransport properties[8–11] at low temperatures. These significant results show the potential of this oxide interface approach for technological applications in nanoelectronics.

LAO consists of alternating $(LaO)^+$ and $(AlO_2)^-$ charge planes while STO consists of $(SrO)^0$ and $(TiO_2)^0$ neutral planes. When LAO is deposited on top of STO, a polar discontinuity can be established at the heterojunction [i.e., $(LaO)^+$ on top of $(TiO_2)^0$]. Hence, the intrinsic doping mechanism underlying this conducting interface is considered to be an electronic reconstruction which could avoid such a "polarization catastrophe."[3,12] However, the perovskite lattice mismatch between LAO and STO is relatively large (about 3%), which can probably hinder the endeavor to approach a high charge carrier mobility within this heterostructure (typically, for LAO/STO interfaces, 10^2-10^3 $cm^2\ V^{-1}\ s^{-1}$ at 4.2 K). In order to effectively tackle this problem and explore the insight of this conducting interface, aside from LAO, other perovskite oxides possessing similar polar (001) atomic planes but low lattice mismatch with STO can be rationally focused.

In this letter, we choose the perovskite $DyScO_3$ (DSO), which has an orthorhombic structure ($GaFeO_3$ type, lattice constants $a=5.440$ Å, $b=5.713$ Å, $c=7.887$ Å) and a perovskite pseudo-cubic lattice constant 3.944 Å. DSO holds the same polarity as LAO, but has a lattice mismatch with STO of less than 1%, resulting in larger critical thickness for strain relaxation. This gives the possibility to fabricate nearly defect-free epitaxial DSO thin films with high quality interfaces. This paper presents electronic properties of such heterointerface grown at different oxygen pressures. In contrast to the insulating property of the DSO/STO interface reported by Luysberg *et al.*,[13] we observed metallic conductivity at the DSO/STO interface. In fact, besides the cations intermixing resulted charge neutrality and therefore the insulating at the interface as reported in Ref. 13, there are a few other reasons made their DSO/STO interface not conducting, such as different substrate used and untreated STO surface etc.

In our work, laser-molecular beam epitaxy with an KrF excimer laser ($\lambda=248$ nm) was used to grow DSO thin films with different thicknesses and under different O_2 pressure conditions (PO_2) on TiO_2-terminated STO single crystal substrate.[14] The deposition temperature was maintained at 750 °C while the oxygen pressure was dynamically controlled between 10^{-6} and 10^{-3} mbar. After deposition, the samples were *in situ* annealed under 10 mbar of O_2 pressure for 1 h at reduced temperature of 400 °C in order to compensate the oxygen vacancies but to avoid the possible intermixing of cations at interfaces. Atomic force microscopy (AFM) and high-resolution transmission electrons microscopy (HRTEM, JEOL JEM 2010) were employed to characterize the qualities of the DSO film surface and the DSO/STO interface. For the transport measurements, platinum contacts to the DSO/STO interface were made with Hall geometry. Keithley source meters combined with a cryogenic stage and Lakeshore Hall measurement system were utilized for the conductivity measurements. For the field effect measurements, a silver electrode was deposited at the back side of the substrate, through which the electric field can be applied to the heterointerface across the dielectric STO.

As shown in Fig. 1(a), the reflective high-energy electron diffraction (RHEED) pattern of the STO substrate at deposition temperature prior to the film growth indicates a perfect crystalline surface.[15] Figure 1(b) is the RHEED pattern of a six-unit-cell DSO layer revealing streaky lines indicating a two-dimensional layer-by-layer growth. The layer-by-layer growth behavior is further confirmed by RHEED intensity oscillation of the specula reflection during growth of DSO. As shown in Fig. 1(c), the total thickness of this

a)Author to whom correspondence should be addressed. Electronic mail: apdaijy@inet.polyu.edu.hk.

 © 2011 American Institute of Physics

Downloaded 14 Feb 2012 to 158.132.161.192. Redistribution subject to AIP license or copyright; see http://apl.aip.org/about/rights_and_permissions

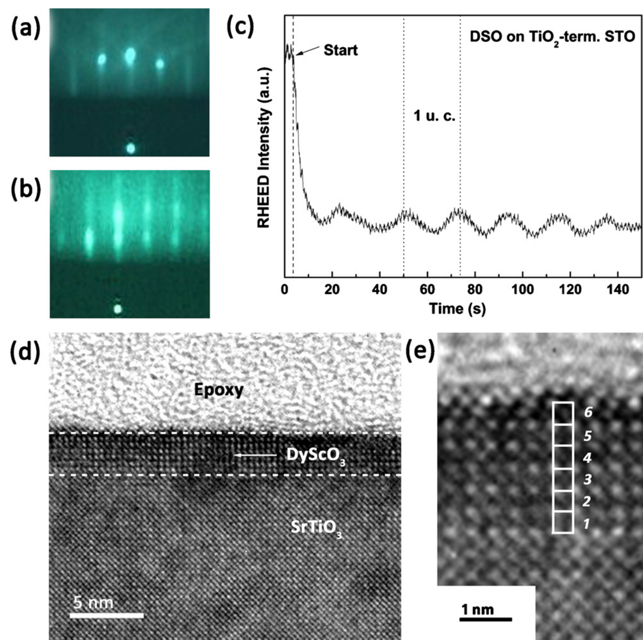

FIG. 1. (Color online) (a) RHEED pattern of TiO_2-terminated $SrTiO_3$ substrate at deposition temperature. (b) RHEED pattern after deposited $DyScO_3$ film for 150 s on $SrTiO_3$. (c) RHEED intensity oscillations during growth of DSO film, indicating a layer-by-layer growth and about six unit cell of DSO were grown on STO. (d) HRTEM image of DSO/STO interface. (e) Magnified image of (d).

DSO layer is determined to be about six unit cells. *Ex situ* AFM proves that the step and terrace structure of the STO surface is preserved after the DSO deposition, confirming the layer-by-layer growth of the DSO layer. One of the six-unit-cell samples was imaged by HRTEM [Fig. 1(d)] confirming the high-quality interface and the thickness estimation from RHEED [Fig. 1(e)].

Figure 2 shows the PO_2 dependence of the transport properties of these DSO/STO samples. The temperature dependence of sheet resistance R_S is given in Fig. 2(a) for the six-unit-cell samples grown at different oxygen pressures. We notice that the room-temperature resistivity increases significantly as the growth oxygen pressure increases. For the samples grown at $PO_2=10^{-6}$ mbar or 10^{-5} mbar, metallic behavior can be observed down to low temperatures, which is similar to the results reported by other groups on LAO/STO interfaces.[16,17] For the sample grown at $PO_2=10^{-4}$ mbar, a resistance upturn presents at temperatures below 90 K. To analyze the mechanism of this metal-to-semiconductor (M–S) transition of the film/interface system, temperature-dependent mobility μ_H was measured from Hall effect [Fig. 2(b)]. We observed that at the M–S transition temperature, about 90 K, μ_H becomes temperature independent, suggesting a drop in the mobile charge carrier density. When PO_2 increases to 10^{-3} mbar, the sample shows obvious insulating behavior. These results reveal that the oxygen pressure PO_2, and thus oxygen vacancies formed in the film and interface, plays an important role in generating this metallic high-mobility electron gas.

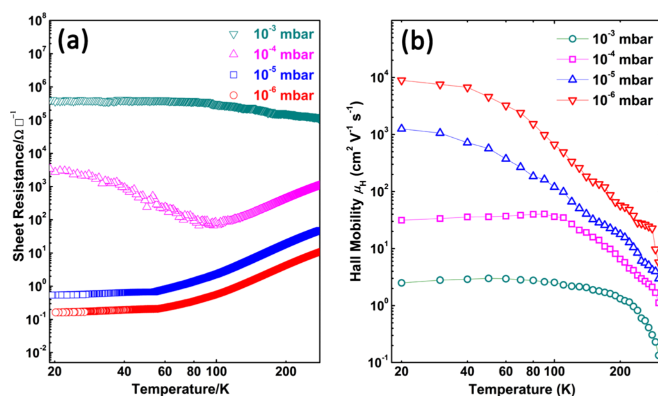

FIG. 2. (Color online) Temperature-dependent sheet resistance (a), and Hall mobility (b), of the DSO/STO interface for the six-unit-cell films grown under different PO_2.

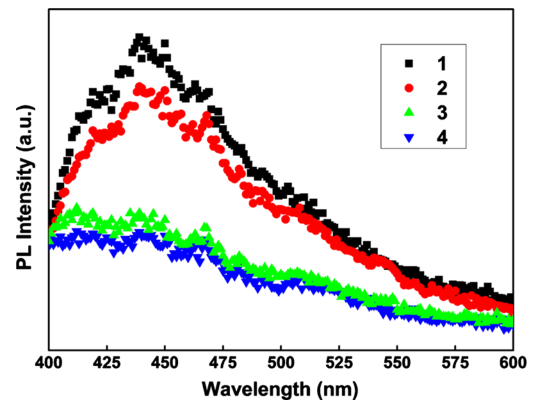

FIG. 3. (Color online) PL intensities of different DSO/STO samples grown under different PO_2 and STO single crystal substrate as a reference: (1) $PO_2=10^{-6}$ mbar; (2) $PO_2=10^{-5}$ mbar; (3) $PO_2=10^{-4}$ mbar; (4) bare STO substrate.

From the Hall measurement of the samples grown under different PO_2, temperature dependence of *n*-type sheet carrier density n_s and the corresponding carrier mobility μ_H were obtained as shown in Fig. 2(b). The Hall mobility can be calculated from equation $\mu_H=-1/n_S R_S e$, where e is the electron charge. The curves in Fig. 2(b) show that for the samples grown under low PO_2 (10^{-6} mbar), carrier mobilities at low temperatures are extremely high, around 10^4 cm^2 V^{-1} s^{-1} below 20 K; and these samples also exhibit a residual resistivity ratio as high as 10^3. Besides, the high sheet carrier density, which is about 10^{17} cm^{-2} (not shown), suggests the presence of oxygen vacancies in STO crystals.[5,17] On one hand, oxygen vacancy induced electrons in the DSO film are injected into the surface layer of STO crystal, i.e., electron doping. On the other hand, much lower lattice mismatch between DSO and STO compared to the LAO/STO results in a lower density of interfacial defects, and therefore, these carriers tolerate much less scattering, and thus, present very high charge carrier mobility.

In order to further understand the oxygen vacancies in the films, photoluminescence (PL) measurements of the DSO films grown under different PO_2 were carried out. The PL spectra, as shown in Fig. 3, show the characteristic peak related to oxygen vacancies, which has the same wavelength and high light intensity as observed by Kalabukhov in the PL spectrum of reduced $SrTiO_3$.[18] However, when PO_2 increases to above 10^{-4} mbar, the corresponding peak reduces to very weak intensity, barely distinguished from the curve of pure STO substrate,[18] implying very low density of oxygen vacancies. These results also demonstrate that DSO layer prevents the oxygen compensation in STO substrate, as also reported by Yuan *et al.*,[19] especially for the samples grown at

Downloaded 14 Feb 2012 to 158.132.161.192. Redistribution subject to AIP license or copyright; see http://apl.aip.org/about/rights_and_permissions

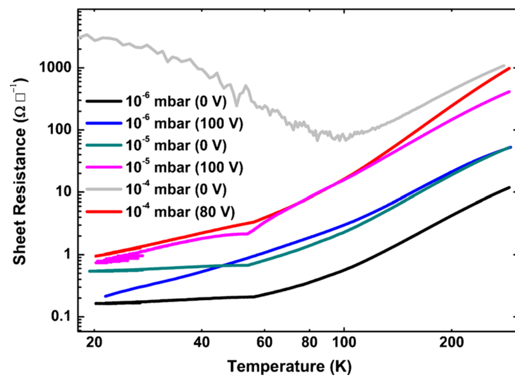

FIG. 4. (Color online) Temperature-dependent sheet resistance for samples applied with different gate voltages (V_G=0, 80, and 100 V).

high vacuum (10^{-6} and 10^{-5} mbar). For the samples grown at $PO_2=10^{-4}$ mbar, the sheet carrier density drops off to approximately 10^{14} cm^{-2} (not shown) which approaches the calculated value from the "polar discontinuity" model (about 3.28×10^{14} cm^{-2}). This may indicate that the high conductivity in the samples grown under high PO_2 is due to the electron gas induced by the polar discontinuity.

In the sample grown under $PO_2=10^{-4}$ mbar condition with low oxygen vacancy density, as mentioned above, an interesting upturn behavior was observed around 90 K in sheet resistance [Fig. 2(a)]. Correspondingly, a maximum appears in the temperature-dependent Hall mobility [Fig. 2(b)] at the same temperature; both of which strongly suggest an M–S transition of the conducting mechanism in this system. This kind of behavior was also found in LAO/STO heterostructures with relatively large LAO thickness,[16,20] for which the LAO films are probably already strain-relaxed and the mechanism is still ambiguous, but rarely observed for such high quality heterointerfaces with highly epitaxial ultrathin (6 uc) films. This phenomenon probably indicates charge localization when the temperature is below 90 K. When temperature decreases at the beginning, significant decrease in sheet resistance due to the less phonon scattering for the free electrons results in a considerable reduction in the temperature-dependent sheet resistance; but when temperature decreases below 90 K, the fact that abundant carriers in semiconductors are restrained and localized in the cryogenic regime should be responsible for the rapid increase in the resistivity of the whole system.

Figure 4 displays the temperature-dependent sheet resistance of different samples applied with different gate voltages. The samples grown under 10^{-6} mbar oxygen partial pressure shows tiny change in sheet resistance under large electric field, indicating a defect-layer originated carrier domination. However, the sample grown under 10^{-5} mbar oxygen partial pressure shows significant change in resistance in one order, implying a strong field effect. Very surprising results came out when we measured the sample presenting M–S transition, where with an applied gate voltage as low as 80 V, the M–S transition disappears and a clear metallic behavior with R_S (280 K)/R_S (20 K)$\sim10^3$ presents. The enormous field effect indicates modulation of the carriers and even quantum phase transition at the interface by field effect. This can be understood by the fact that, the polar catastrophe caused band bending can be drastically affected by the electric field, where relatively large electric field provokes large band bending resulting in more free electrons injected to STO conduction band and dominate the conductivity at the interface. The fact, that the free electrons at the interfaces are extremely sensitive to electric field, enables us to modulate M–S transition by applying an external electric field. This result is significant because, we can not only control the doping level originated from the electronic reconstruction but also change the interface quantum state through the electrical means. Therefore, this heterostructure promises the potential interest for understanding q2-DEGs as well as its applications in all-oxide device.

This project is supported by Hong Kong GRF Grant (Grant No. POLYU5006/09P). We thank J. H. Hao for providing $DyScO_3$ target.

[1] J. Mannhart and D. G. Schlom, Science **327**, 1607 (2010).
[2] S. B. Ogale, *Thin Films and Heterostructures for Oxide Electronics* (Springer, New York, 2005), Chap. 5.
[3] A. Ohtomo and H. Y. Hwang, Nature (London) **427**, 423 (2004).
[4] S. Thiel, G. Hammerl, A. Schmehl, C. W. Schneider, and J. Mannhart, Science **313**, 1942 (2006).
[5] M. Basletic, J. L. Maurice, C. Carrétéro, G. Herranz, O. Copie, M. Bibes, E. Jacquet, K. Bouzehouane, S. Fusil, and A. Barthélémy, Nature Mater. **7**, 621 (2008).
[6] O. Copie, V. Garcia, C. Bodefeld, C. Carretero, M. Bibes, G. Herranz, E. Jacquet, J.-L. Maurice, B. Vinter, S. Fusil, K. Bouzehouane, H. Jaffres, and A. Barthelemy, Phys. Rev. Lett. **102**, 216804 (2009).
[7] N. Reyren, S. Thiel, A. D. Caviglia, L. F. Kourkoutis, G. Hammerl, C. Richter, C. W. Schneider, T. Kopp, A. S. Ruetschi, D. Jaccard, M. Gabay, D. A. Muller, J. M. Triscone, and J. Mannhart, Science **317**, 1196 (2007).
[8] S. Seri and L. Klein, Phys. Rev. B **80**, 181410(R) (2009).
[9] M. Ben Shalom, C. W. Tai, Y. Lereah, M. Sachs, E. Levy, D. Rakhmilevitch, A. Palevski, and Y. Dagan, Phys. Rev. B **80**, 140403(R) (2009).
[10] M. Ben Shalom, M. Sachs, D. Rakhmilevitch, A. Palevski, and Y. Dagan, Phys. Rev. Lett. **104**, 126802 (2010).
[11] A. D. Caviglia, M. Gabay, S. Gariglio, N. Reyren, C. Cancellieri, and J. M. Triscone, Phys. Rev. Lett. **104**, 126803 (2010).
[12] N. Nakagawa, H. Y. Hwang, and D. A. Muller, Nature Mater. **5**, 204 (2006).
[13] M. Luysberg, M. Heidelmann, L. Houben, M. Boese, T. Heeg, J. Schubert, and M. Roeckerath, Acta Mater. **57**, 3192 (2009).
[14] M. Kawasaki, K. Takahashi, T. Maeda, R. Tsuchiya, M. Shinohara, O. Ishiyama, T. Yonezawa, M. Yoshimoto, and H. Koinuma, Science **266**, 1540 (1994).
[15] G. J. H. M. Rijnders, G. Koster, D. H. A. Blank, and H. Rogalla, Appl. Phys. Lett. **70**, 1888 (1997).
[16] A. Brinkman, M. Huijben, M. Van Zalk, J. Huijben, U. Zeitler, J. C. Maan, W. G. Van der Wiel, G. Rijnders, D. H. A. Blank, and H. Hilgenkamp, Nature Mater. **6**, 493 (2007).
[17] G. Herranz, M. Basletic, M. Bibes, C. Carretero, E. Tafra, E. Jacquet, K. Bouzehouane, C. Deranlot, A. Hamzic, J. M. Broto, A. Barthelemy, and A. Fert, Phys. Rev. Lett. **98**, 216803 (2007).
[18] A. Kalabukhov, R. Gunnarsson, J. Borjesson, E. Olsson, T. Claeson, and D. Winkler, Phys. Rev. B **75**, 121404(R) (2007).
[19] G. L. Yuan, K. Nishio, M. Lippmaa, and A. Uedono, J. Phys. D: Appl. Phys. **43**, 025301 (2010).
[20] C. Bell, S. Harashima, Y. Hikita, and H. Y. Hwang, Appl. Phys. Lett. **94**, 222111 (2009).

Downloaded 14 Feb 2012 to 158.132.161.192. Redistribution subject to AIP license or copyright; see http://apl.aip.org/about/rights_and_permissions